

Anomalous Size Effect of Pt Ultrathin Nanowires on Oxygen Reduction Reaction

Zhaoyu Yao,[○] Yuliang Yuan,[○] Tao Cheng,[○] Lei Gao,[○] Tulai Sun, Yangfan Lu, Yi-Ge Zhou,*
Pedro L. Galindo, Zhilong Yang, Liang Xu, Hao Yang, and Hongwen Huang*



Cite This: *Nano Lett.* 2021, 21, 9354–9360



Read Online

ACCESS |

Metrics & More

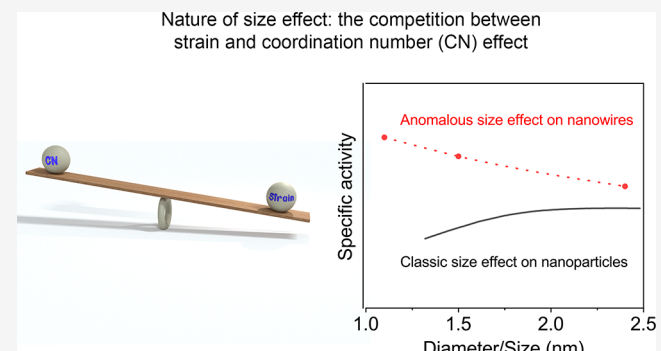
Article Recommendations

Supporting Information

ABSTRACT: The classical size effect of Pt particles on oxygen reduction reaction (ORR) suggests that the activity and durability would decrease with reducing the particle size, self-limiting the effectiveness in maximizing the Pt utilization efficiency with the particle-size-reduction strategy. Herein, we discover an anomalous size effect based on Pt nanowires (NWs) with tunable diameters, where the monotonically increasing activity and durability for ORR were observed with decreasing the diameter from 2.4 to 1.1 nm. Our results reveal that the dominant role of increased compressive strain induced by decreasing the diameter of NWs in weakening the adsorption and suppressing the Pt dissolution accounts for this anomalous size effect, where the reduced low-coordinated sites on NWs, the intrinsic structural advantage, is the root. Our findings not only expand the knowledge to the classical size effect but also provide new implications to break through the size limit in the design of Pt-based ORR catalysts.

KEYWORDS: anomalous size effect, diameter-dependent, oxygen reduction, platinum, strain

Proton-exchange membrane fuel cells (PEMFCs) with hydrogen as the fuel is considered as a pivotal technology to curb our reliance on fossil fuels due to the inherent advantages of high energy efficiency and zero-emission.^{1–3} However, the industrial-scale deployment of such technology is currently impeded by the use of a large amount of precious Pt on the cathode to accelerate the kinetically slow oxygen reduction reaction (ORR). As thus, increasing the utilization efficiency (UE) of Pt to reduce the usage is of great importance. Presently, the most extensively used strategy to increase the UE of Pt is the reduction of particle size.^{4,5} However, as described by the well-established size effect of Pt nanoparticles (NPs) for ORR, the specific activity of Pt NPs would decrease with particle-size reduction due to the increased proportion of low-coordinated Pt sites that strongly bind oxygenated species.^{5–8} Besides, the smaller particles tend to aggregate or sinter into larger ones during the long-term operation, causing a more severe loss in mass activity.^{9–12} These negative impacts on specific activity and durability have thus set a ceiling for the use of the strategy in improving the UE of Pt. On this account, the state-of-the-art commercial Pt/C catalyst is practically made of NPs with diameters typically in the range of 2.0 to 3.0 nm.¹³ Based on the analysis, breaking through the size limit to earn new room for the further increment of UE is mightily desired, especially given the extensive use of this strategy in practice.

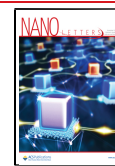


Very recently, Pt-based ultrathin nanowires (NWs) have emerged as promising catalysts for ORR because of their advantages in simultaneously achieving high UE, high specific activity, and long-term durability.^{13–19} Basically, the remarkable activity and durability of Pt-based NWs were reasonably ascribed to the favored geometrical structure and optimal compositions, which optimize the electronic structure and reinforce the resistance to the sintering process. Impressively, the diameters of the Pt-based NWs had been pushed down to 1 nm in those prior studies, which are already located in the deteriorate region of the NPs system. A fundamental question thus lies here: why the Pt NWs seemingly have the lower size limit for ORR performance? Undoubtedly, understanding the knowledge of the size effect on Pt NWs may give some implications for catalyst design. However, there is the absence of an ideal model catalyst to probe this information at present, given the previous work mainly focusing on the adjustment of composition.

Received: October 5, 2021

Revised: October 27, 2021

Published: November 1, 2021



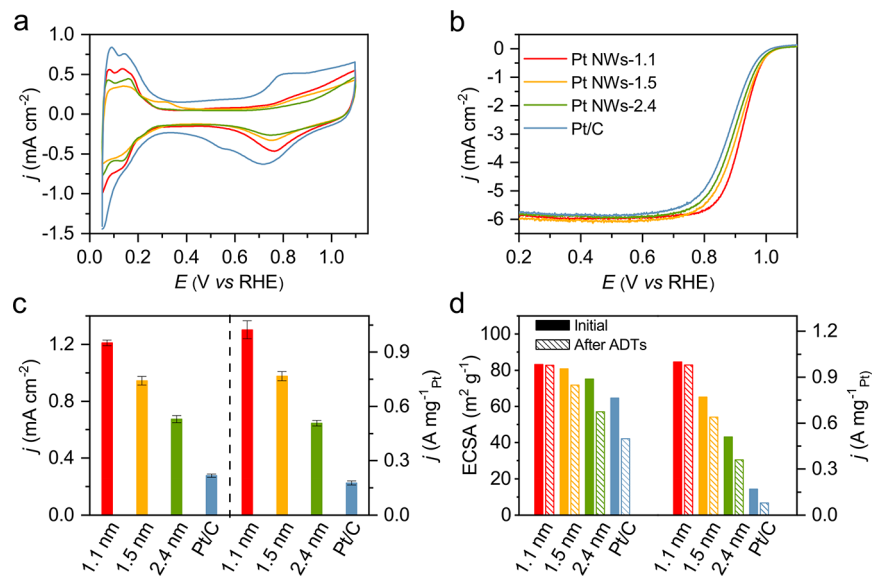


Figure 1. ORR performance of Pt NWs with different diameters. (a) Cyclic voltammograms recorded at room temperature in a N_2 -purged 0.1 M HClO_4 solution with a sweep rate of 50 mV s^{-1} . (b) Corresponding positive-going ORR polarization curves recorded in an O_2 -saturated 0.1 M HClO_4 solution with a sweep rate of 10 mV s^{-1} and a rotation rate of 1600 rpm. (c) The comparison of specific activity and mass activity at $0.9 \text{ V}_{\text{RHE}}$. (d) The changes in the ECSA and mass activities before and after 10,000 cycles of ADTs. The color scheme in panel b applies to all other panels.

On the basis of the above analysis, we herein delicately design a set of ideal model catalysts by tuning the diameter of Pt NWs in the range of 1.1–2.4 nm and systematically investigate their diameter-dependent ORR performance. Strikingly, the Pt NWs with ultrathin diameters exhibited a monotonic activity and durability improvement with the decrease of Pt NWs down to 1.1 nm, showing the anomalous diameter-dependent ORR performance compared with Pt NPs. The origin for this anomalous diameter-dependent ORR behavior is further worked out by combining the experimental analyses and computational simulations.

Results and Discussion. Diameter-Dependent ORR Performance. To investigate the diameter-dependent ORR performance of Pt NWs, we first synthesized the Pt NWs with tunable diameters as the model catalysts by slightly modifying the synthetic procedures (see Supporting Information for details). The morphologies of Pt NWs with different diameters were examined by TEM. As shown in Figures S1–S3, the diameters were determined as 1.1, 1.5, and 2.4 nm via statistic counting (hereafter, we noted these NWs as Pt NWs-1.1, Pt NWs-1.5, and Pt NWs-2.4 for convenience, respectively). The carbon-supported catalysts were then prepared by loading the as-synthesized Pt NWs on Vulcan-72 carbon under ultrasonication with Pt contents of 20 wt %. TEM images of as-prepared Pt NWs/C catalysts indicate the uniform dispersions of Pt NWs on carbon supports (Figure S4a–d). To exclude the possible impacts from the surfactants on the ORR performance, the treatments by heating the catalysts in concentrated acetic acid (99.5%) solution were conducted to remove the surfactants on the surface of Pt NWs. The clean surface of the catalysts after post-treatment was confirmed by FTIR, where almost no signal of CTAB or DDAB can be detected (Figures S5 and S6). In this case, these NW catalysts can be served as idea models for unraveling the effect of diameter on ORR performance.

For ORR measurements, the cyclic voltammograms (CVs) of NW catalysts were first recorded in N_2 -saturated 0.1 M

HClO_4 at a scan rate of 50 mV s^{-1} (Figure 1a). The electrochemical active surface areas (ECSAs) of the catalysts were then estimated from the charges of hydrogen adsorption/desorption in the potential range of 0.05 and $0.35 \text{ V}_{\text{RHE}}$. Consistent with the variation tendency of diameter, the Pt NWs-1.1 exhibited an ECSA of $83.1 \text{ m}^2 \text{ g}^{-1}$, much greater than those of Pt NWs-1.5 ($80.8 \text{ m}^2 \text{ g}^{-1}$), Pt NWs-2.4 ($75.2 \text{ m}^2 \text{ g}^{-1}$), and commercial Pt/C ($64.6 \text{ m}^2 \text{ g}^{-1}$). The polarization curves were subsequently recorded in O_2 -saturated 0.1 M HClO_4 solution with a positive-going scan at a rotation rate of 1600 rpm (Figure 1b), then the kinetic currents of catalysts were calculated based on the Koutecky–Levich equation. As shown in Figure 1c, a monotonically increasing activity for ORR is observed with the decrease of diameter. Specifically, the Pt NWs-1.1 showed the highest specific activity of 1.20 mA cm^{-2} at $0.9 \text{ V}_{\text{RHE}}$, which is 1.26-, 1.76-, and 4.62-fold higher than that of Pt NWs-1.5 (0.95 mA cm^{-2}), Pt NWs-2.4 (0.68 mA cm^{-2}), and commercial Pt/C (0.26 mA cm^{-2}), respectively. Due to both improved Pt utilization efficiency and specific activity, an amplified effect is expected for the mass activities of NW catalysts. As depicted in Figure 1c, the Pt NWs-1.1 displayed a mass activity of 1.00 A mg^{-1} at $0.9 \text{ V}_{\text{RHE}}$, which is 1.30, 1.96, and 5.88 times higher than that of Pt NWs-1.5 (0.77 A mg^{-1}), Pt NWs-2.4 (0.51 A mg^{-1}), and the commercial Pt/C (0.17 A mg^{-1}), respectively.

The effect of diameter on long-term catalytic durability was also investigated for different NWs via an accelerated durability test (ADT). After ADTs, the polarization curves of NW catalysts were recorded (Figures S7–S10), whereas the mass activities were estimated. As shown in Figure 1d, the mass activity of Pt NWs-1.1 only exhibited a drop of 2.7% after 10,000 cycles, whereas big decreases of 16.7%, 29.0%, and 54.0% were observed on Pt NWs-1.5, Pt NWs-2.4, and commercial Pt/C catalysts, respectively. We further examined the changes in ECSA and morphology of different NW catalysts after 10,000 cycles. Agreeing with the trend in durability, the Pt NWs-1.1 well maintained the ECSA and

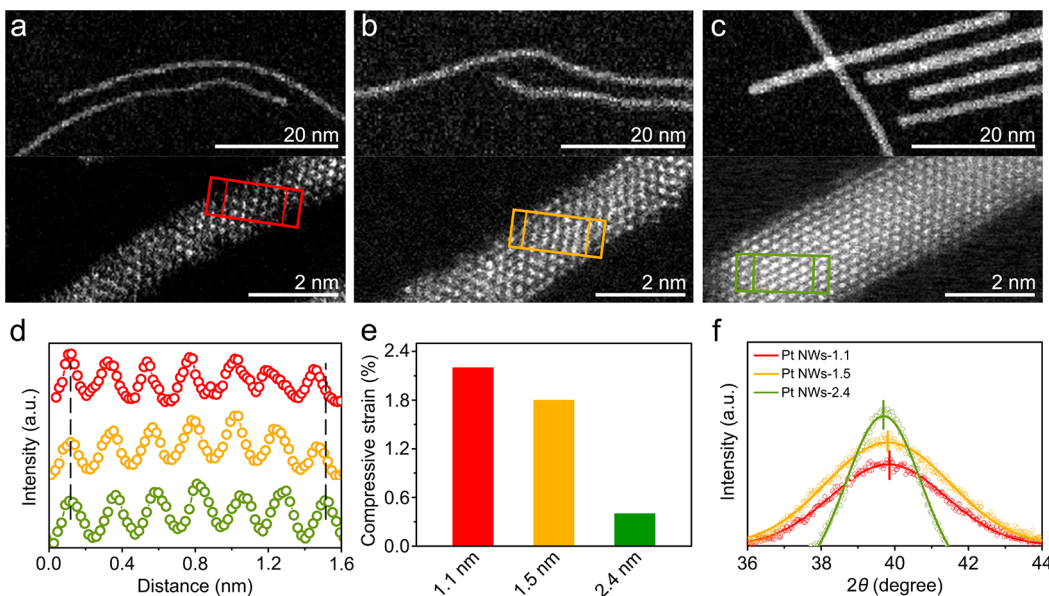


Figure 2. Structural analysis. HAADF-STEM images of (a) Pt NWs-1.1, (b) Pt NWs-1.5, and (c) Pt NWs-2.4. (d) The intensity profiles of Pt NWs recorded from the enlarged images in panels a–c. (e) Compressive strains of Pt NWs with different diameters. (f) XRD patterns of Pt NWs with different diameters. The color scheme in panel f applies to all other panels.

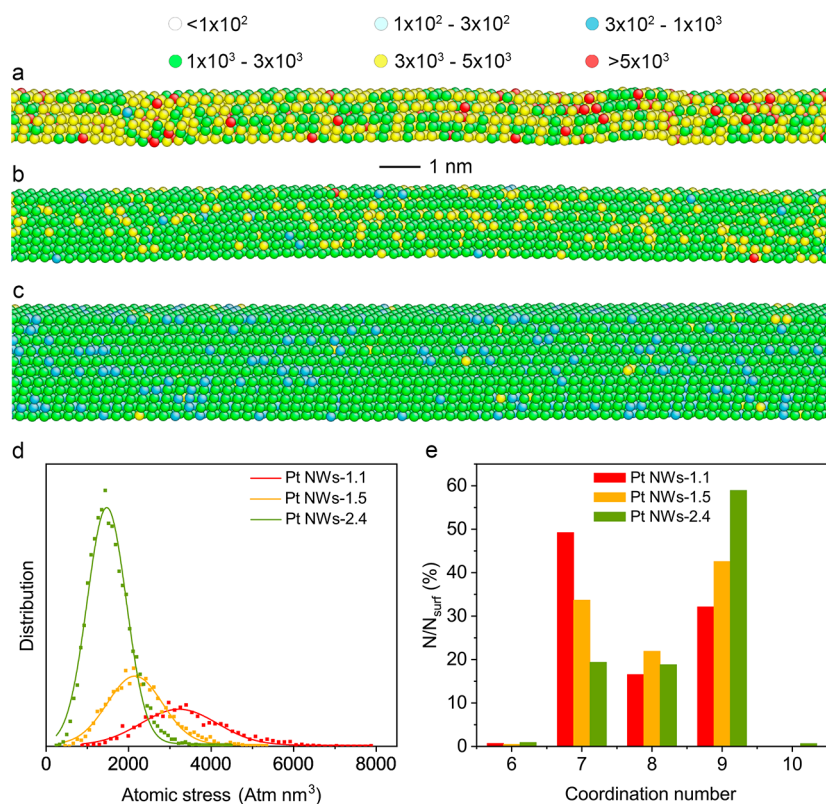


Figure 3. RMD simulations. (a–c) Models of the Pt NWs with different diameters. (d) Distributions of the absolute values of the atomic stress on the surface of Pt NWs with different diameters. (e) Distributions of the coordination number for Pt NWs with different diameters.

morphology compared to other NW catalysts after 10,000 cycles of ADTs (Figure 1d and Figure S4e–h). Moreover, the ex situ ICP measurement revealed that the dissolution of Pt NWs-1.1 is significantly smaller than that of the benchmark Pt/C catalyst (Figure S11). These results clearly indicate that the NWs with thinner diameters showed better structural stability and catalytic durability.

According to the classical theory of size effect for ORR, the specific activity and durability of Pt NPs would decrease with the decrease of particle size.⁵ Intriguingly, we herein observed an entirely different size-dependent ORR performance on Pt ultrathin NWs where the ORR performance improves with the decrease of diameter. It should be noted that such an anomalous relationship between diameter and ORR performance means the Pt NWs have inherent advantages in

simultaneously achieving high Pt utilization efficiency and specific activity.

Structural Analysis. Figure 2a–c shows the uniform one-dimensional Pt NWs with distinguishable diameter differences. The interplanar spacings of (111) planes in the atomic-resolved images were then measured as 2.26 Å for Pt NWs-2.4, 2.23 Å for Pt NWs-1.5, and 2.22 Å for Pt NWs-1.1 (Figure 2d). Compared to the bulk single crystal of Pt (2.27 Å for (111) interplanar distance), the NWs showed compressive strains of 0.4%, 1.8%, and 2.2%, respectively (Figure 2e). Furthermore, the X-ray diffraction (XRD) patterns of NWs presented that the diffraction peaks shifted toward higher diffraction angle with decreasing the diameter of NWs (Figure 2f and Figure S12), verifying the compressive strain increases with the reduction of the diameter. It should be mentioned that the compressive strain on these ultrathin NWs is likely related to the surface contraction, which is driven by the reduction of surface energy.²⁰

To further analyze the lattice strain on Pt NWs, we conducted reactive molecular dynamics (RMD) to simulate the strain distribution.^{21–23} To obtain a more accurate analysis, we built three kinds of Pt NW models (Figure 3a–c) with very similar diameters to the as-synthesized NWs and applied reactive force field (ReaxFF) for their local optimization (see the molecular dynamic calculation section in Supporting Information for details). The simulated strain distribution showed that the thinner NWs have the larger and denser compressive strain (Figure 3a), agreeing well with the results from HAADF-STEM and XRD. The atomic stress distribution profiles of three NWs in Figure 3d further quantitatively confirmed the variation trend in compressive strain on the NWs. Overall, the combination of microscopic analysis and RDM simulations both demonstrated that the increased compressive strain would appear with decreasing the diameter of NWs.

In addition, the coordination number of surface atoms is the other factor to alter the ORR activity of Pt NWs by impacting the adsorption strength. Because it is difficult to examine the coordination number of surface Pt atoms on NWs using an experimental technique, a common neighbor analysis based on the models constructed for Pt NWs-1.1, Pt NWs-1.5, and Pt NWs-2.4 was performed to extract the information on coordination number.^{24–26} As shown in Figure 3e, the thinner Pt NWs have more low-coordinated sites with the coordination number of 7 (corresponding to the edge site). Taking all of the structural analysis, we thus concluded that decreasing the diameter of NWs would increase the compressive strain and number of low-coordinated sites simultaneously.

Understanding the Anomalous Diameter-Dependent ORR Performance. As the electronic structure of catalyst intrinsically determines the catalytic activity,^{27–29} we probed the surface electronic structures of Pt NWs by combining the experimental techniques of surface valence band photoemission spectrum and CO-stripping voltammetry to rationalize the anomalous diameter-dependent ORR activity.^{30–38} As shown in Figure 4a, a monotonic downshift of the d-band center with the decrease of diameter was observed from the surface valence band photoemission spectra of the NWs. Based on the well-established d-band theory, the downshifted d-band center would decrease the adsorption energies of oxygenated species and thus result in the improved ORR activity given the too strong binding on Pt.³⁹ The variation tendency of electronic structure for Pt NWs was also confirmed by a

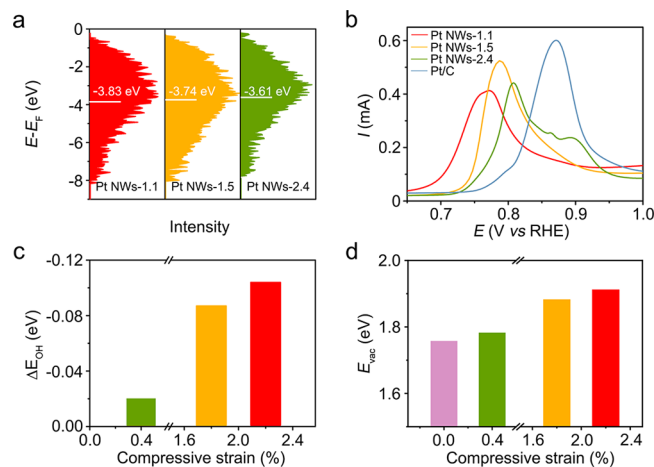


Figure 4. Understanding of anomalous diameter-dependent ORR performance. (a) Surface valence band spectra of Pt NWs with different diameters. (b) CO stripping voltammetric curves of Pt NWs with different diameters. (c) ΔE_{OH} as a function of compressive strain. (d) E_{vac} as a function of compressive strain (the light purple bar denotes the Pt(111) slab without strain). The color scheme in panel b applies to all other panels.

monotonic negative shift in onset potential for CO electro-oxidation with the decrease of diameters shown in Figure 4b. Note that there is more than one peak of CO stripping for Pt NWs-2.4, which, we speculate, is the additional stripping on the end-sites of Pt NWs due to the increased proportion of end-sites on the shorter Pt NWs-2.4 (Figure S3). Overall, both of these pieces of evidence indicated that decreasing the diameter of Pt NWs may downshift the d-band center, self-consistent with the observed activity trends.

We further attempted to understand why the thinner NWs have the lower d-band center. Because the atomic structure of NWs determines the electronic structure, we examined the effects of compressive strain and low-coordinated sites, the key structural features determined by the diameter of NWs, on the electronic structure and ORR activity. The impacts of compressive strain on the electronic structure and adsorption energy of key intermediate were first evaluated by density functional theory (DFT) calculations. Since Pt (111) surface is thermodynamically stable, Pt (111) slabs with different compressive strains as models were constructed (Figure S13). As shown in Figure S14, the calculated d-band center exhibited a monotonic downshift from 0.4% strained Pt slab to 2.2% strained Pt slab, agreeing well with the result from XPS valence band spectra. The adsorption energy of OH, an effective descriptor for ORR activity,^{40,41} on the slab was further analyzed as displayed in Figure 4c. Specifically, the ΔE_{OH} (defined as the difference of adsorption energy between the strained Pt (111) slab and unstrained Pt (111) slab) on Pt (111) slabs with compressive strains of 0.4%, 1.8%, and 2.2% are 0.02, 0.087, and 0.104 eV, respectively. According to the previous studies, the optimal adsorption energy of OH is 0.1 eV weaker than that on unstrained Pt (111) slab.⁴⁰ The calculations on adsorption energy thus suggested that the specific activity increases with increasing the compressive strain. In addition to the lattice strain, we also analyzed the roles of the increased proportion of low-coordinated sites in the electronic structure and specific activity of NWs. In principle, the catalytic site with a low coordination number would elevate the d-band center and thus strengthen the

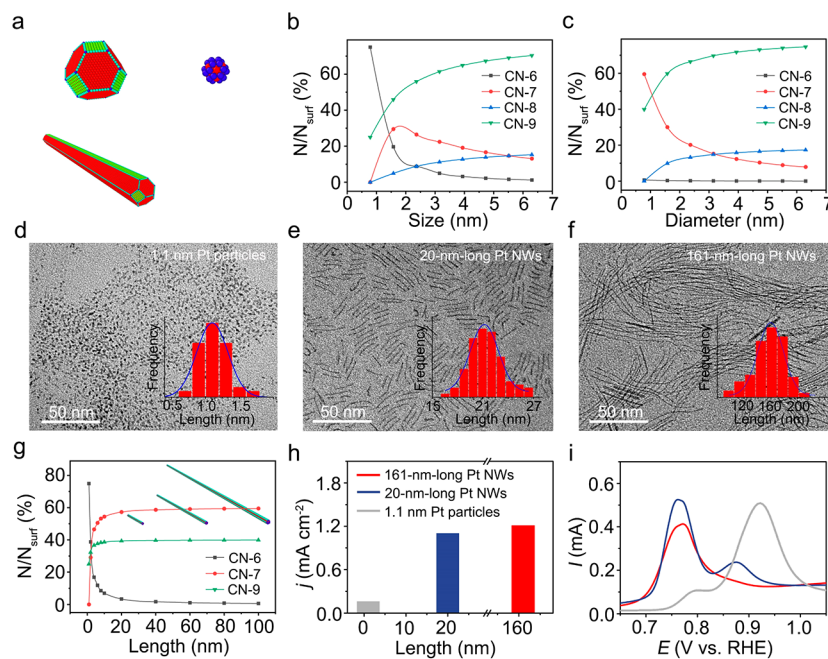


Figure 5. Analysis on the difference in the surface structures for Pt NWs and NPs. (a) The models of Pt NPs and Pt NWs with different sizes/diameters. The surface coordination number distribution (described as N/N_{surf}) for (b) Pt NPs and (c) Pt NWs with different sizes/diameters. TEM images of (d) 1.1 nm long Pt NWs (or NPs), (e) 20 nm long Pt NWs, and (f) 161 nm long Pt NWs (insets show the histogram of length distribution). (g) The surface coordination number distribution for Pt NWs with different lengths (insets show the models of Pt NWs with different lengths). (h) ORR performance for Pt NWs with different lengths. (i) CO-stripping voltammograms for Pt NWs with different lengths.

chemisorption.²⁶ This means that decreasing the diameter of NWs would cause two opposite effects on the electronic structure. As a result, the competition between the compressive strain and low-coordinated sites would eventually govern the electronic structure and specific activity of NWs. On the basis of these analyses, we could reasonably figure out that the increased compressive strain induced by decreasing the diameter of NWs dominated the change in the electronic structure of Pt ultrathin NWs, causing the downshifted d-band center and improved specific activity for ORR.

Besides, we also assessed the influence of compressive strain on the catalytic stability of NWs by comparing the Pt vacancy formation energy (E_{vac}), an indicator to describe the resistance to Pt dissolution, on the three Pt slabs.^{42,43} As shown in Figure 4d, increasing the compressive strain leads to an increased E_{vac} , which suggests that the compressive strain would suppress the Pt dissolution and thus improve the stability of Pt catalyst for ORR. Given that the catalytic sites with lower coordination numbers would have faster dissolution kinetics due to their higher Gibbs free energy, it is reasonable to conjecture that the compressive strain is the dominant factor to determine the stability of Pt ultrathin NWs. Taking all of these analyses together, the essence of anomalous diameter-dependent ORR performance can be traced back to the dominant role of the compressive strain induced by decreasing the diameter in weakening the adsorption and suppressing the Pt dissolution.^{13–17}

The above results further raised an essential question that what's the root for the different dominant factors in determining the ORR performance for Pt NWs and NPs, which should be tracked back to the intrinsic differences in their surface structures. Because the microscopic techniques have limited ability to analyze the surface structure of NWs, we carried out the coordination number distribution analysis for

surface atoms of NWs and NPs with different diameters/sizes based on the simulations. A series of atomic models for Pt NPs with perfect cuboctahedral shape⁴⁴ and Pt NWs by extending perfect cuboctahedra along $\langle 110 \rangle$ direction to a length of 100 nm were then constructed (Figure 5a and Figures S15–S17). For NPs, when the size decreases from 6.3 to 0.8 nm, the percentage of sites with the coordination number of 9 (CN-9 sites) decreases from 70.3% to 25.0%, and the percentage of sites with the coordination number of 6 (CN-6 sites) increases from 1.2% to 75.0% (Figure 5b). Whereas for NWs (Figure 5c), the percentage of CN-9 sites decreases from 74.7% to 39.9%, while the percentage of CN-6 sites remains almost unchanged (from 0.08% to 0.67%). These results clearly showed that the NWs could largely reduce the proportion of low-coordinated sites when compared with the NPs, which may rationalize the fact that the strain effect outweighs the effect of low-coordinated sites for NWs. This interpretation is assumed to be the intrinsic difference between NWs and NPs. Experimentally, we also designed a set of experiments to verify the hypothesis by varying the distributions of surface sites on NWs. Specifically, we decreased the reaction time during the synthesis of Pt NWs-1.1, and hence obtained 16, 20, and 1.1 nm (namely, NPs) long Pt NWs with the same diameter (Figure 5d–f). Since the reduction of length gradually increases the ratio of low-coordinated sites (Figure 5g), it is expected a decrease of specific activity would occur. Indeed, there is a small decrease of specific activity during the length reduction from 161 to 20 nm (Figure 5h), in accordance with the small increase of CN-6 sites (Figure 5g). The more obvious decrease of specific activity was observed with the length reduced from 20 to 1.1 nm, which is well consistent with the dramatic increase of sites with CN-6 below 20 nm. In addition, CO stripping was employed to investigate the surface properties of Pt NWs with different lengths (Figure 5i).

Notably, the 161 nm long Pt NWs exhibited a single potential peak at 0.772 V_{RHE}, whereas 20 nm long Pt NWs exhibited a shoulder potential peak at 0.87 V_{RHE}. This shoulder peak, which originated from the low-coordinated end-sites of NWs that bind CO stronger than the side-sites, is raised due to the increased ratio of end-sites with the decrease of length. With a further decrease of NWs' length, the finally obtained Pt NPs exhibited a single CO stripping peak positive than 0.90 V_{RHE}, which corresponds to the strong CO adsorption sites (Figure S1). This self-consistent evidence confirmed the increased proportion of low-coordinated sites during the transformation from Pt NWs to Pt NPs. Also, the variations in adsorption strength agreed with the observed trend in ORR performance of Pt NWs with different lengths. Overall, the largely reduced proportion of low-coordinated sites on NWs, the intrinsic structural advantage, is the root for the anomalous size effect. In conclusion, we have constructed the model catalyst based on Pt NWs with controllable diameters ranging from 1.1 to 2.4 nm to elucidate the diameter-dependent ORR performance on Pt NWs. Strikingly, an anomalous size effect of Pt ultrathin NWs on ORR was found, where the monotonically increasing activity and durability for ORR were observed with decreasing the diameter from 2.4 to 1.1 nm. A combination of structural characterizations and MD simulations indicated that decreasing the diameter would simultaneously increase the compressive strain and proportions of low-coordinated sites. The mechanistic analyses further revealed the dominant role of increased compressive strain induced by decreasing the diameter of NWs in weakening the adsorption and suppressing the Pt dissolution is the underlying reason for this anomalous size effect, where the reduced low-coordinated sites on NWs, the intrinsic structural advantage, is the root.

■ ASSOCIATED CONTENT

SI Supporting Information

The Supporting Information is available free of charge at <https://pubs.acs.org/doi/10.1021/acs.nanolett.1c03805>.

Experimental details; TEM images; XPS; FT-IR spectra of all Pt-based NWs; CV and LSV curves of the long-term durability test; theoretical model structures; d-band projected density states; a table of MA, SA, and ECSA (PDF)

■ AUTHOR INFORMATION

Corresponding Authors

Yi-Ge Zhou – College of Chemistry and Chemical Engineering, Hunan University, Changsha, Hunan 410082, P. R. China; orcid.org/0000-0002-4155-7222; Email: yigezhou@hnu.edu.cn

Hongwen Huang – College of Materials Science and Engineering, Hunan University, Changsha, Hunan 410082, P. R. China; Hefei National Laboratory for Physical Sciences at the Microscale, University of Science and Technology of China, Hefei, Anhui 230026, P. R. China; orcid.org/0000-0003-3967-6182; Email: huanghw@hnu.edu.cn

Authors

Zhaoyu Yao – College of Materials Science and Engineering, Hunan University, Changsha, Hunan 410082, P. R. China

Yuliang Yuan – College of Materials Science and Engineering, Hunan University, Changsha, Hunan 410082, P. R. China

Tao Cheng – Institute of Functional Nano & Soft Materials, Soochow University, Suzhou, Jiangsu 215123, P. R. China; orcid.org/0000-0003-4830-177X

Lei Gao – College of Materials Science and Engineering, Hunan University, Changsha, Hunan 410082, P. R. China

Tulai Sun – Center for Electron Microscopy, State Key Laboratory Breeding Base of Green Chemistry Synthesis Technology and College of Chemical Engineering, Zhejiang University of Technology, Hangzhou, Zhejiang 310014, P. R. China

Yangfan Lu – State Key Lab of Silicon Materials, School of Materials Science and Engineering, Zhejiang University, Hangzhou 310027, P. R. China; orcid.org/0000-0002-5260-6835

Pedro L. Galindo – Department of Computer Engineering, University de Cadiz, Cadiz, Andalusia 11510, Spain

Zhilong Yang – College of Materials Science and Engineering, Hunan University, Changsha, Hunan 410082, P. R. China

Liang Xu – Institute of Functional Nano & Soft Materials, Soochow University, Suzhou, Jiangsu 215123, P. R. China

Hao Yang – Institute of Functional Nano & Soft Materials, Soochow University, Suzhou, Jiangsu 215123, P. R. China; orcid.org/0000-0002-8241-6231

Complete contact information is available at:

<https://pubs.acs.org/10.1021/acs.nanolett.1c03805>

Author Contributions

○Z.Y., Y.Y., T.C., and L.G. contributed equally to this work.

Notes

The authors declare no competing financial interest.

■ ACKNOWLEDGMENTS

This work was supported by the National Natural Science Foundation of China (U2032149 and 21905089), the Hunan Provincial Natural Science Foundation of China (2020JJ3001, 2020JJ5041, and 2020JJ5043), the Hefei National Laboratory for Physical Sciences at the Microscale (KF2020108), and Fundamental Research Funds for the Central Universities.

■ REFERENCES

- (1) Barbir, F. *PEM Fuel Cells: Theory and Practice* 2013, 1–518.
- (2) Debe, M. K. Electrocatalyst Approaches and Challenges for Automotive Fuel Cells. *Nature* 2012, 486, 43–51.
- (3) Banham, D.; Ye, S. Current Status and Future Development of Catalyst Materials and Catalyst Layers for Proton Exchange Membrane Fuel Cells: An Industrial Perspective. *ACS Energy Lett.* 2017, 2, 629–638.
- (4) Kinoshita, K. Particle Size Effects for Oxygen Reduction on Highly Dispersed Platinum in Acid Electrolytes. *J. Electrochem. Soc.* 1990, 137, 845–848.
- (5) Shao, M.; Peles, A.; Shoemaker, K. Electrocatalysis on Platinum Nanoparticles: Particle Size Effect on Oxygen Reduction Reaction Activity. *Nano Lett.* 2011, 11, 3714–3719.
- (6) Mayrhofer, K. J.; Blizanac, B. B.; Arenz, M.; Stamenkovic, V. R.; Ross, P. N.; Markovic, N. M. The Impact of Geometric and Surface Electronic Properties of Pt-Catalysts on the Particle Size Effect in Electrocatalysis. *J. Phys. Chem. B* 2005, 109, 14433–14440.
- (7) Wang, D.; Liu, Z. P.; Yang, W. M. Revealing the Size Effect of Platinum Cocatalyst for Photocatalytic Hydrogen Evolution on TiO₂ Support: A Dft Study. *ACS Catal.* 2018, 8, 7270–7278.
- (8) Guo, J.; Gao, L.; Tan, X.; Yuan, Y.; Kim, J.; Wang, Y.; Wang, H.; Zeng, Y. J.; Choi, S. I.; Smith, S. C.; Huang, H. Template-Directed Rapid Synthesis of Pd-Based Ultrathin Porous Intermetallic Nano-

- sheets for Efficient Oxygen Reduction. *Angew. Chem., Int. Ed.* **2021**, *60*, 10942–10949.
- (9) Hansen, T. W.; Delariva, A. T.; Challa, S. R.; Datye, A. K. Sintering of Catalytic Nanoparticles: Particle Migration or Ostwald Ripening? *Acc. Chem. Res.* **2013**, *46*, 1720–1730.
- (10) Plessow, P. N.; Abild-Pedersen, F. Sintering of Pt Nanoparticles Via Volatile PtO₂: Simulation and Comparison with Experiments. *ACS Catal.* **2016**, *6*, 7098–7108.
- (11) Tabib Zadeh Adibi, P.; Pingel, T.; Olsson, E.; Grönbeck, H.; Langhammer, C. Pt Nanoparticle Sintering and Redispersion on a Heterogeneous Nanostructured Support. *J. Phys. Chem. C* **2016**, *120*, 14918–14925.
- (12) Zhang, J.; Yuan, Y.; Gao, L.; Zeng, G.; Li, M.; Huang, H. Stabilizing Pt-Based Electrocatalysts for Oxygen Reduction Reaction: Fundamental Understanding and Design Strategies. *Adv. Mater.* **2021**, *33*, 2006494.
- (13) Huang, H.; Li, K.; Chen, Z.; Luo, L.; Gu, Y.; Zhang, D.; Ma, C.; Si, R.; Yang, J.; Peng, Z.; Zeng, J. Achieving Remarkable Activity and Durability toward Oxygen Reduction Reaction Based on Ultrathin Rh-Doped Pt Nanowires. *J. Am. Chem. Soc.* **2017**, *139*, 8152–8159.
- (14) Gao, L.; Li, X.; Yao, Z.; Bai, H.; Lu, Y.; Ma, C.; Lu, S.; Peng, Z.; Yang, J.; Pan, A.; Huang, H. Unconventional P-D Hybridization Interaction in PtGa Ultrathin Nanowires Boosts Oxygen Reduction Electrocatalysis. *J. Am. Chem. Soc.* **2019**, *141*, 18083–18090.
- (15) Li, K.; Li, X.; Huang, H.; Luo, L.; Li, X.; Yan, X.; Ma, C.; Si, R.; Yang, J.; Zeng, J. One-Nanometer-Thick PtNiRh Trimetallic Nanowires with Enhanced Oxygen Reduction Electrocatalysis in Acid Media: Integrating Multiple Advantages into One Catalyst. *J. Am. Chem. Soc.* **2018**, *140*, 16159–16167.
- (16) Li, M.; Zhao, Z.; Cheng, T.; Fortunelli, A.; Chen, C. Y.; Yu, R.; Zhang, Q.; Gu, L.; Merinov, B. V.; Lin, Z.; Zhu, E.; Yu, T.; Jia, Q.; Guo, J.; Zhang, L.; Goddard, W. A., III; Huang, Y.; Duan, X. Ultrafine Jagged Platinum Nanowires Enable Ultrahigh Mass Activity for the Oxygen Reduction Reaction. *Science* **2016**, *354*, 1414–1419.
- (17) Jiang, K.; Zhao, D.; Guo, S.; Zhang, X.; Zhu, X.; Guo, J.; Lu, G.; Huang, X. Efficient Oxygen Reduction Catalysis by Subnanometer Pt Alloy Nanowires. *Sci. Adv.* **2017**, *3*, e1601705.
- (18) Bu, L.; Guo, S.; Zhang, X.; Shen, X.; Su, D.; Lu, G.; Zhu, X.; Yao, J.; Guo, J.; Huang, X. Surface Engineering of Hierarchical Platinum-Cobalt Nanowires for Efficient Electrocatalysis. *Nat. Commun.* **2016**, *7*, 11850.
- (19) Bu, L.; Ding, J.; Guo, S.; Zhang, X.; Su, D.; Zhu, X.; Yao, J.; Guo, J.; Lu, G.; Huang, X. A General Method for Multimetallic Platinum Alloy Nanowires as Highly Active and Stable Oxygen Reduction Catalysts. *Adv. Mater.* **2015**, *27*, 7204–7012.
- (20) Wang, L.; Zeng, Z.; Gao, W.; Maxson, T.; Raciti, D.; Giroux, M.; Pan, X.; Wang, C.; Greeley, J. Tunable Intrinsic Strain in Two-Dimensional Transition Metal Electrocatalysts. *Science* **2019**, *363*, 870–874.
- (21) Cleri, F.; Rosato, V. V. Tight-Binding Potentials for Transition Metals and Alloys. *Phys. Rev. B: Condens. Matter Mater. Phys.* **1993**, *48*, 22–33.
- (22) Sanz-Navarro, C. F.; Astrand, P. O.; Chen, D.; Ronning, M.; van Duin, A. C.; Jacob, T.; Goddard, W. A., III Molecular Dynamics Simulations of the Interactions between Platinum Clusters and Carbon Platelets. *J. Phys. Chem. A* **2008**, *112*, 1392–1402.
- (23) Fortunelli, A.; Goddard, W. A., III; Sementa, L.; Barcaro, G.; Negreiros, F. R.; Jaramillo-Botero, A. The Atomistic Origin of the Extraordinary Oxygen Reduction Activity of Pt₃Ni₇ Fuel Cell Catalysts. *Chem. Sci.* **2015**, *6*, 3915–3925.
- (24) Honeycutt, J. D.; Andersen, H. C. Molecular Dynamics Study of Melting and Freezing of Small Lennard-Jones Clusters. *J. Phys. Chem.* **1987**, *91*, 4950–4963.
- (25) Faken, D.; Jónsson, H. Systematic Analysis of Local Atomic Structure Combined with 3d Computer Graphics. *Comput. Mater. Sci.* **1994**, *2*, 279–286.
- (26) Schnur, S.; Groß, A. Strain and Coordination Effects in the Adsorption Properties of Early Transition Metals: A Density-Functional Theory Study. *Phys. Rev. B: Condens. Matter Mater. Phys.* **2010**, *81*, 033402.
- (27) Stamenković, V.; Mun, B. S.; Mayrhofer, K. J. J.; Ross, P. N.; Markovic, N. M.; Rossmeisl, J.; Greeley, J.; Nørskov, J. K. Changing the Activity of Electrocatalysts for Oxygen Reduction by Tuning the Surface Electronic Structure. *Angew. Chem.* **2006**, *118*, 2963–2967.
- (28) Escudero-Escribano, M.; Malacrida, P.; Hansen, M. H.; Vej-Hansen, U. G.; Velazquez-Palenzuela, A.; Tripkovic, V.; Schiotz, J.; Rossmeisl, J.; Stephens, I. E.; Chorkendorff, I. Tuning the Activity of Pt Alloy Electrocatalysts by Means of the Lanthanide Contraction. *Science* **2016**, *352*, 73–76.
- (29) Wang, H.; Xu, S.; Tsai, C.; Li, Y.; Liu, C.; Zhao, J.; Liu, Y.; Yuan, H.; Abild-Pedersen, F.; Prinz, F. B.; Nørskov, J. K.; Cui, Y. Direct and Continuous Strain Control of Catalysts with Tunable Battery Electrode Materials. *Science* **2016**, *354*, 1031–1036.
- (30) Hammer, B.; Morikawa, Y.; Nørskov, J. K. CO Chemisorption at Metal Surfaces and Overlayers. *Phys. Rev. Lett.* **1996**, *76*, 2141–2144.
- (31) Ciapina, E. G.; Santos, S. F.; Gonzalez, E. R. Electrochemical CO Stripping on Nanosized Pt Surfaces in Acid Media: A Review on the Issue of Peak Multiplicity. *J. Electroanal. Chem.* **2018**, *815*, 47–60.
- (32) Shao, M.; Odell, J. H.; Choi, S.-I.; Xia, Y. Electrochemical Surface Area Measurements of Platinum- and Palladium-Based Nanoparticles. *Electrochim. Commun.* **2013**, *31*, 46–48.
- (33) Liu, P.; Nørskov, J. K. Ligand and Ensemble Effects in Adsorption on Alloy Surfaces. *Phys. Chem. Chem. Phys.* **2001**, *3*, 3814–3818.
- (34) Gao, F.; Goodman, D. W. Pd-Au Bimetallic Catalysts: Understanding Alloy Effects from Planar Models and (Supported) Nanoparticles. *Chem. Soc. Rev.* **2012**, *41*, 8009–8020.
- (35) Shirley, D. A. High-Resolution X-Ray Photoemission Spectrum of the Valence Bands of Gold. *Phys. Rev. B* **1972**, *5*, 4709–4714.
- (36) Mun, B. S.; Watanabe, M.; Rossi, M.; Stamenkovic, V.; Markovic, N. M.; Ross, P. N., Jr. A Study of Electronic Structures of Pt₃M (M = Ti, V, Cr, Fe, Co, Ni) Polycrystalline Alloys with Valence-Band Photoemission Spectroscopy. *J. Chem. Phys.* **2005**, *123*, 204717.
- (37) Jørgensen, M.; Grönbeck, H. Strain Affects CO Oxidation on Metallic Nanoparticles Non-Linearly. *Top. Catal.* **2019**, *62*, 660–668.
- (38) Panaccione, G.; Cautero, G.; Cautero, M.; Fondacaro, A.; Grioni, M.; Lacovig, P.; Monaco, G.; Offi, F.; Paolicelli, G.; Sacchi, M.; Stojic, N.; Stefani, G.; Tommasini, R.; Torelli, P. High-Energy Photoemission in Silver: Resolving d and sp Contributions in Valence Band Spectra. *J. Phys.: Condens. Matter* **2005**, *17*, 2671–2679.
- (39) Greeley, J.; Stephens, I. E.; Bondarenko, A. S.; Johansson, T. P.; Hansen, H. A.; Jaramillo, T. F.; Rossmeisl, J.; Chorkendorff, I.; Nørskov, J. K. Alloys of Platinum and Early Transition Metals as Oxygen Reduction Electrocatalysts. *Nat. Chem.* **2009**, *1*, 552–556.
- (40) Nørskov, J. K.; Rossmeisl, J.; Logadottir, A.; Lindqvist, L.; Kitchin, J. R.; Bligaard, T.; Jónsson, H. Origin of the Overpotential for Oxygen Reduction at a Fuel-Cell Cathode. *J. Phys. Chem. B* **2004**, *108*, 17886–17892.
- (41) Kulkarni, A.; Siahrostami, S.; Patel, A.; Nørskov, J. K. Understanding Catalytic Activity Trends in the Oxygen Reduction Reaction. *Chem. Rev.* **2018**, *118*, 2302–2312.
- (42) Alahmed, Z.; Fu, H. First-Principles Determination of Chemical Potentials and Vacancy Formation Energies in PbTiO₃ and BaTiO₃. *Phys. Rev. B: Condens. Matter Mater. Phys.* **2007**, *76*, 224101.
- (43) Yu, X.; Zhan, Z.; Rong, J.; Liu, Z.; Li, L.; Liu, J. Vacancy Formation Energy and Size Effects. *Chem. Phys. Lett.* **2014**, *600*, 43–45.
- (44) Le Valant, A.; Comminges, C.; Can, F.; Thomas, K.; Houalla, M.; Epron, F. Platinum supported catalysts: predictive CO and H₂ chemisorption by a statistical cuboctahedron cluster model. *J. Phys. Chem. C* **2016**, *120*, 26374–26385.